Modelling of detailed subject-specific FE rib models for fracture prediction

Johan Iraeus[1], Linus Lundin[2], Simon Storm[2], Bengt Pipkorn[3]

[1] Chalmers University of Technology, Sweden
[2] ÅF Industry, Sweden
[3] Autoliv Development, Sweden

Keywords –

Human Body Model, Finite element, Rib, Subject specific model, Fracture prediction

Abstract –

Traditionally, anthropometric test devices have been used to evaluate occupant injury risk in car crashes. In recent years, as a complement, there is also an increased use of detailed finite element (FE) human body model. Such models can be used to evaluate injury on tissue level, for example fracture of single ribs. Previous efforts to create subject specific rib models for fracture prediction, using different meshing strategies, have shown mixed results. Therefore, the aim of this study is to evaluate if the ANSA hexa-box meshing approach can be used to create subject specific all-hexahedral FE human rib models of high quality and to evaluate if these models can predict fracture location in anterior-posterior rib bending.

High resolution clinical computed tomography (CT) data was used to generate detailed subject-specific geometry for twelve FE rib models. The rib cortex inner and outer surfaces were estimated using a cortical bone mapping algorithm. After initial smoothing, hexa-boxes were fitted to the rib geometry. A pure hexahedral mesh was created for each rib, consisting of 0.61 to 1.53 million elements. The FE ribs were then positioned in a FE model of the test fixture and subjected to the same anterior-posterior rib bending as in the physical tests. Rib fracture location was estimated as the position for the element with highest maximum principle strain at the time corresponding to rib fracture in the physical test

The quality for the all-hex solid mesh was compared to published recommendations. For most ribs, less than 5% of the elements had an aspect ratio over three, and a maximum internal angle deviating more than 45° from the ideal angle. In addition, less than 1% of the elements had a Jacobian below 0.7.

For six out of the twelve ribs the model predicted the fracture locations. It is hypothesis that the difference between two groups can be attributed to differences in cortical bone structure, e.g. intracortical porosity, on a level that is not captured in high resolution clinical CT.

This study provides guidelines for future FE modelling of human ribs.

Introduction

Traditionally, anthropometric test devices (ATDs), also called crash test dummies, have been used to evaluate occupant injury risk in car crashes. In recent years, as a complement, there is also an increased use of detailed finite element (FE) human body models (HBMs). Such models can be used to evaluate injury on tissue level, for example fracture of single ribs.

Previous efforts to create subject specific rib models for fracture prediction, have shown mixed results. Charpail et al. (2005) performed anterior posterior bending tests on 30 human ribs. Four out of these were modelled based on clinical CT scans, using a combination of 4-noded thin shells and 8-noded solids. The authors found correspondence between the simulation predictions and actual fracture locations. In another study, using a similar test setup and FE modelling approach, Li et al. (2010b) reproduced four subject specific ribs. The FE models all predicted laterally located fractures, while only one of the physical ribs fractured at the lateral aspect. In a follow-up study, Li et al. (2010a), modelled three out of these ribs in great detail using an octree-based all-hexahedral mesh. The all-hexahedral mesh predicted the fracture location for two of the three ribs, thus showing slightly better performance compared to rib models using a combination of thin shells and solids.

The geometry of many human body parts, e.g. the ribs, are challenging from a FE modelling point of view. The rib geometry has a beam like shape, where the posterior (rear) end is connected to the spine, and the anterior (front) end is connected to the costal cartilage. Along the length of the rib, the cross section shape and dimensions, as well as the thickness of the outer shell (the cortex), varies. The ribs are also curved in two dimensions. In particular the costal groove, a thin protruding structure, protecting the intercostal vein, arteries, and nerve, makes FE modelling challenging.

The first aim of this study is to evaluate if ANSA hexa-box meshing approach can create all-hexahedral FE human rib models of high quality. The second aim is to evaluate if subject specific FE rib models, using high quality hex-mesh, based on state-of-the-art clinical CT data can predict rib stiffness and fracture location in anterior-posterior rib bending.

Method

This study is based on twelve sixth level ribs, previously tested in an anterior-posterior rib bending configuration, at The Ohio State University. More details are given in Agnew et al. (2018). Prior to testing the rib geometries were captured using high resolution clinical computed tomography CT (Philips Ingenuity 64-slice), with in-plane resolution 0.146mm and slice thickness 0.625mm. The periosteal (outer) and endosteal (inner) surfaces of the rib cortexes were estimated using a cortical bone mapping (CBM) algorithm, Holcombe et al. (2018). The resulting surfaces after the CBM process needed smoothing, see Figure 1 (left).The ANSA function *Suppress > Noise*, with intensity factor set to *local peaks (ultra low)*, *Move only nodes*, was used for the smoothing. This resulted in a surface more appropriate for FE meshing, see Figure 1 (right).
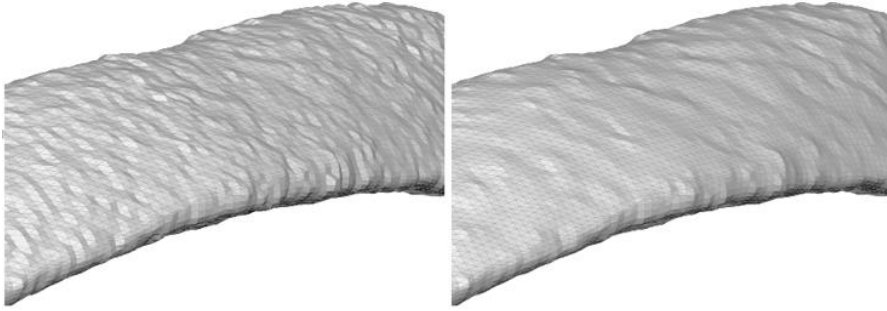
Figure 1. Resulting CAD surface from CBM before smoothing (left) and after smoothing (right)

The rib cortex, i.e. the volume in-between the periosteal and the endosteal surfaces varies both in shape and thickness along the rib, see Figure 2 for an example. Even more challenging is the variation in shape of the volume inside the endosteal surface representing the trabecular bone.
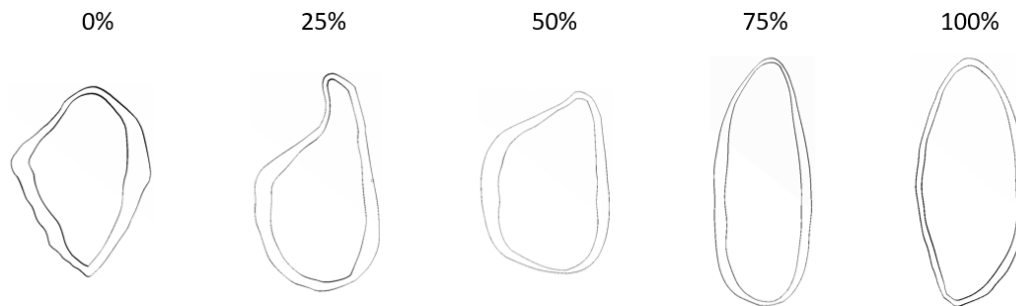
Figure 2. Variation in cortex geometry. 0% represent most posterior end (at the spine) and 100% represent most anterior end (at the costal cartilage.

It was judged that the best meshing approach for this complex geometry was the semi-automatic Hexa-Block method. First, Hexa-boxes were created and projected onto the endosteal surface, creating a volume definition for the trabecular bone. These boxes were then split sufficiently many times to capture the variation in cross section shape and the resulting cross-sectional edges were projected onto the endosteal surface, see Figure 3.
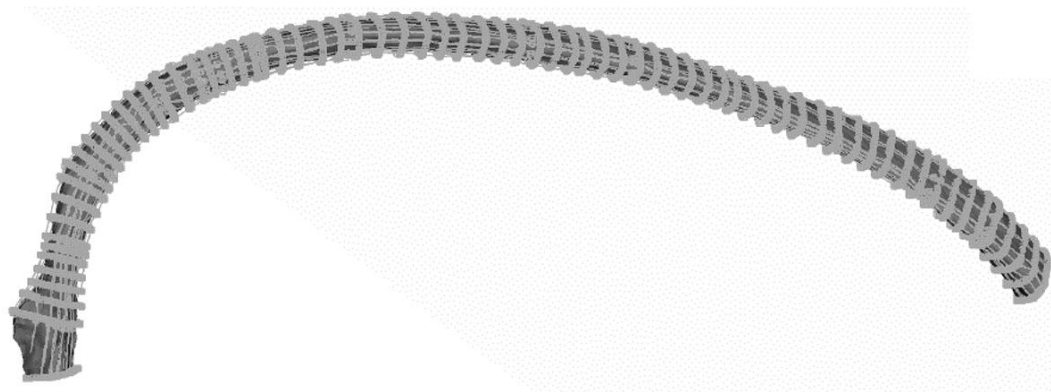
Figure 3. Endosteal surface with Hexa-Boxes.

In the next step, the outer faces of the Hexa-boxes were offset outwards, with subsequent fitting to the periosteal surface, to create a volume definition for the cortex. Finally, the hexa-boxes were filled with a pure hexahedral mesh. To capture local bending over the cortex, this was modelled with three elements over the thickness. The complete meshing strategy and an example of the final mesh can be seen in Figure 4. LS-DYNA solid element formulation one, with hourglass definition type five was used for all rib elements, LSTC (2015). An isotropic material model was used for the cortex, and non-linear, subject specific material data was created based on subject specific tensile coupon test. The linear material properties for the trabecular bone was based on a regression model relating Young's modulus to the bone density, using the 3D Image Segmentation and Processing Software ScanIP [Simpleware LTD (2017)].

| Endosteal surface | Trabecular solids | Periosteal surface | Cortex solids | | Periosteal and endosteal surface | Cortex and trabecular solids |
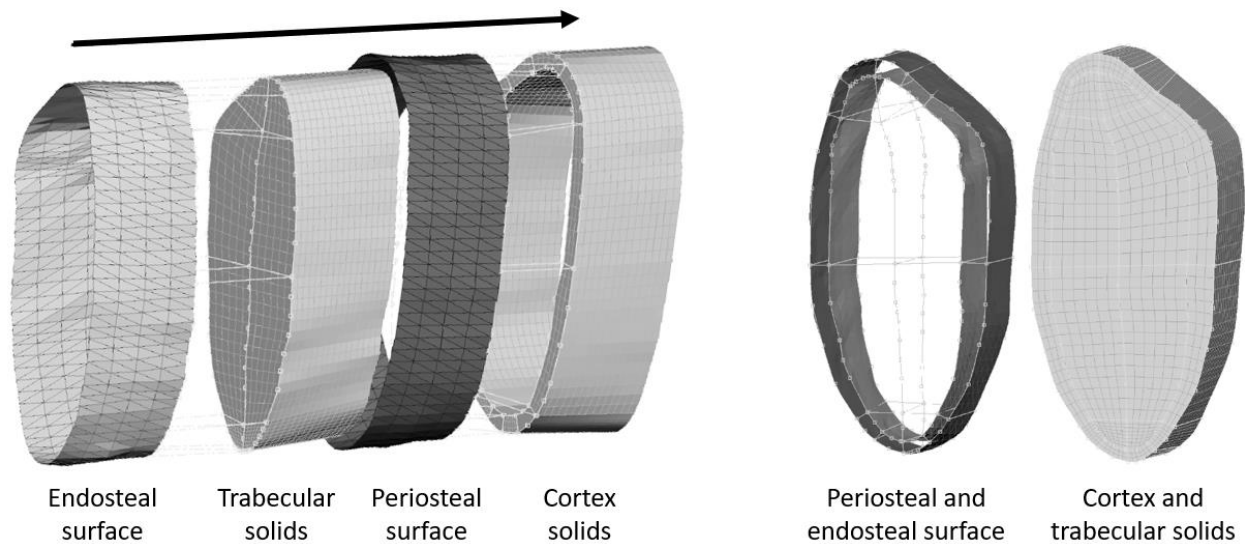
Figure 4. Complete meshing strategy, following the arrow from left to right. An example of the hexa-boxes and the final mesh is shown to the right.

Each of the 12 modelled ribs were positioned in the FE model of the test rig seen in Figure 5. The rib ends were constrained to the rib pots. The rib pots lower surfaces were constrained to the potting brackets, which in turn was attached to the support and load components using rotational joints, only allowing the brackets to rotate around the z-axis. The anterior load component was given a prescribed displacement, identical to what was measured for each rib in the physical tests. The reaction force was measured at the posterior support component, which was fixed in space. To evaluate the FE model rib kinematics and kinetics accuracy, rib reaction forces and potting bracket rotations were compared to the physical tests results. Finally, rib fracture location in the FE models were estimated as the position for the elements with highest maximum principal strain. To make the evaluation robust to numerical noise the top 27 elements were selected and highlighted. Within a solid of pure hexahedral elements, picking the element with highest strain, and then adding all adjacent elements will result in 27 elements, as long as the peak strain element is not located on the surface. Finally, the location of these elements were compared to the actual location of the fracture.
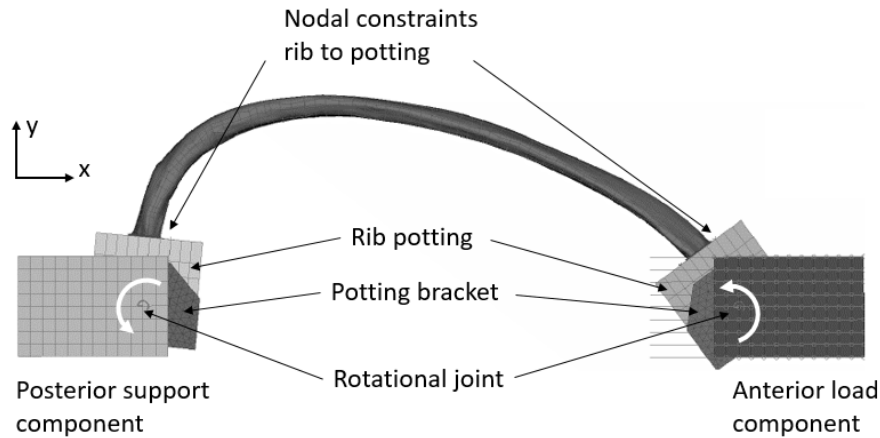
Figure 5. Anterior-posterior rib bending test setup.

All pre-processing was performed in ANSA version 18.1.1 (BETA CAE Systems, Switzerland) and the simulations were run in LS-DYNA MPP version 9.2 (LSTC, Livermore, CA). Post processing was performed in META version 18.1.1 (BETA CAE Systems, Switzerland) and MATLAB version 2018s (Mathworks, Natick, MA).

Results

The mesh quality of the hexahedral elements is shown in Table 1. According to Burkhart et al. (2013), less than 5% of the elements should have an aspect ratio larger than 3 and no elements should have an aspect ratio above 10. Except ribs K, L, and G this was fulfilled. In addition, no more than 5% of the elements should have internal angles deviating more than 45° from the ideal angle, and no internal angles should deviate more than 70°. The mesh do not fully fulfill these criteria, but it is close. Finally, less than 5% of the elements should have a Jacobian less than 0.7, which was fulfilled for all the meshes. It should be noted that ribs K and L were modelled using an O-grid pattern for the trabecular volume. This modelling approach was inferior for this application, and subsequent ribs were modelled using another element pattern. The number of elements ranged from 614,000 to 1,530,000 for each ribs. The average element side length varies between ribs from 0.21mm and 0.33mm.

Table 1. Rib mesh details and fulfillment of element quality criteria.

Rib	#Elements	AR>3	AR>10	Angle 90±45	Angle 90±70	Jacobian≤0.7
A	1,530,000	4%	0.01%	6%	0.5%	0%
B	1,350,000	2%	0.00%	8%	0.8%	0%
C	1,130,000	5%	0.01%	4%	0.4%	0%
D	945,000	5%	0.01%	8%	0.7%	0%
E	646,000	4%	0.00%	5%	1.2%	0%
F	859,000	5%	0.01%	4%	0.5%	0%
G	740,000	7%	0.01%	4%	0.5%	0%
H	719,000	3%	0.02%	5%	0.7%	0%
I	825,000	3%	0.00%	4%	0.7%	0%
J	1,380,000	5%	0.03%	7%	0.5%	0%
K	614,000	25%	0.05%	9%	1.0%	0%
L	1,130,000	22%	0.6%	7%	0.1%	0.1%

The fracture location predicted by the FE models is compared to the actual fracture locations in

Table 2. The circle(s) marks the area(s) for the 27 elements with highest maximum principle strain, at the time for fracture in the physical ribs. In some ribs the peak strain is distributed over an area, resulting in several circles. The fracture locations for the actual ribs are marked with a jagged line. For six of the ribs, the predicted fracture location is close to the actual location. For some of the other ribs the actual fracture location is far from any strain localization. Rib I is a special case as the FE model shows a small band of thin cortex resulting in a strain localization. It is hypothesized that this is an artifact of the CT scan or CBM process, and not actually a physical property of the actual rib.

Table 2. Comparison of predicted fracture location (circles) to actual fracture location (jagged line). The fringe is set showing red areas for strains above 1.75% (except for rib I where it is above 2.63%).

Rib	Fracture location estimation	Accurate
A		NO
B		YES
C		NO
D		NO
E		YES
F		YES
G		NO
H		YES
I		NO
J		YES
K		YES
L		NO
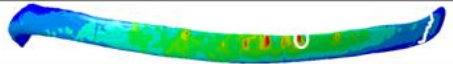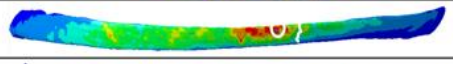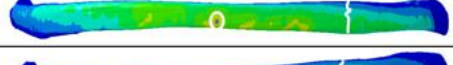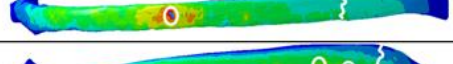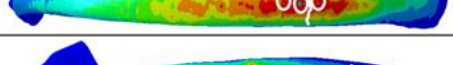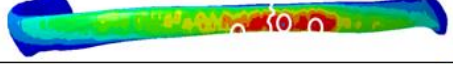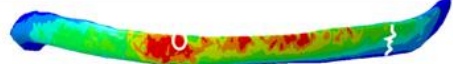
Discussion

The Hexa-block meshing procedure used in this study, produced rib meshes of high quality. For the trabecular bone, it was also shown that a regular mesh pattern gave elements of higher quality compared to an O-grid mesh pattern. The aspect ratio criteria together with the requirement of using three elements of the thickness of the cortex, showed to be a major restriction on the lengthwise element size. Another mesh-related challenge was that for some ribs, the protruding structure at the

costal groove was quite thin, effectively squeezing the element of the trabecular bone together. It was mainly in this region the O-grid mesh pattern performed inferior to the regular mesh pattern.

The actual rib fracture location is most likely sensitive to local imperfections. The medical image technique used for this study have a native in-plane resolution of 0.146mm. This is about one fourth of the average cortex thickness of the ribs in this study. The imperfections, intracortical pores or micro cracks, are typically on a much smaller scale. The CBM algorithm is only determining the inner and outer surface of the cortex, i.e. it does not consider intracortical pores. Further, the CBM rib cortex thickness prediction accuracy, was shown to be -0.03±0.17mm, for high resolution CT scans in Holcombe et al. (2018). This means that for areas with thin cortex, the standard deviation of the thickness estimation is in the same order as the actual thickness, potentially leading to large relative errors of the cortex thickness estimation.

It has been shown that the rib cortex area decrease with age [Sedlin et al. (1963), Epker et al. (1965), Takahashi and Frost (1966), and Stein and Granik (1976)]. Comparing the average thickness of the rib cortex for the rib models showing an accurate prediction of the fracture location with the others (except Rib I, which is considered as an outlier) shows that the first group had an average thickness of 0.68mm and the latter 0.59mm. The decrease in cortex thickness is often associated with an increase in porosity. McCalden et al. (1993) showed that cortical bone porosity increased with age, and that this change in porosity accounts for 76% of the reduction in material tensile strength. The existence of pores or micro cracks in the actual rib will give local stress concentrations that are not captured in the current FE model. These stress concentrations can lead to fractures in areas of low nominal stress.

FE rib models consisting of millions of solid elements, cannot practically be used in whole body HBMs, partly due to the Courant-Friedrich-Lewy condition, restricting the time step in the explicit time integration, and partly due to the sheer number of elements. Future studies should focus on model simplifications, e.g. mesh coarsening, that can be done without losing predictability.

Conclusion

This study shows that Hexa-block meshing can be used to create high quality all hexahedral solid meshes of human ribs. Further, this study indicates that rib fracture location can be predicted using maximum principle strain, for detailed subject specific all-hexahedral rib models, subjected to simplified anterior-posterior bending, for ribs with cortex of sufficient thickness and quality. These results provides guidelines for future FE modelling of human ribs.

References

Agnew AM, Murach MM, Dominguez VM, et al. Sources of Variability in Structural Bending Response of Pediatric and Adult Human Ribs in Dynamic Frontal Impacts. *Stapp Car Crash J.* Nov 2018;62:119-192.

Burkhart TA, Andrews DM, Dunning CE. Finite element modeling mesh quality, energy balance and validation methods: a review with recommendations associated with the modeling of bone tissue. *Journal of biomechanics.* 2013;46(9):1477-1488.

Charpail E, Trosseille X, Petit P, Laporte S, Lavaste F, Vallancien G. Characterization of PMHS Ribs: A New Test Methodology. *Stapp Car Crash Journal.* 2005;49:183.

Epker B, Kelin M, Frost H. Magnitude and location of cortical bone loss in human rib with aging. *Clinical orthopaedics and related research.* 1965;41:198-203.

Holcombe SA, Hwang E, Derstine BA, Wang SC. Measuring rib cortical bone thickness and cross section from CT. *Medical Image Analysis.* 2018;49:27-34.

Li Z, Kindig MW, Kerrigan JR, et al. Rib fractures under anterior–posterior dynamic loads: experimental and finite-element study. *Journal of Biomechanics.* 2010a;43(2):228-234.

Li Z, Kindig MW, Subit D, Kent RW. Influence of mesh density, cortical thickness and material properties on human rib fracture prediction. *Medical Engineering & Physics.* 2010b;32(9):998-1008.

LS-DYNA Keyword User's Manual [computer program]. Livermore, California, US: Livermore Software Technonlgy Corporation; 2015.

McCalden R, McGeough J, Barker M. Age-related changes in the tensile properties of cortical bone. The relative importance of changes in porosity, mineralization, and microstructure. *J Bone Joint Surg Am.* 1993;75(8):1193-1205.

Sedlin ED, Frost HM, Villanueva AR. Variations in cross-section area of rib cortex with age. *Journal of gerontology.* 1963;18(1):9-13.

Simpleware Reference Guide [computer program]. Innovation centre rennes drive, Exeter, United Kingdom: Simpleware LTD; 2017.

Stein I, Granik G. Rib structure and bending strength: an autopsy study. *Calcified tissue research.* 1976;20(1):61-73.

Takahashi H, Frost HM. Age and sex related changes in the amount of cortex of normal human ribs. *Acta Orthopaedica Scandinavica.* 1966;37(2):122-130.